



Article

The Efficiency of Calcium Oxide on Microbial Self-Healing Activity in Alkali-Activated Slag (AAS)

Nancy Hammad ¹, Amr El-Nemr ^{1,2}  and Ibrahim G. Shaaban ^{3,*} 

¹ Civil Engineering Department, German University in Cairo (GUC), New Cairo 11835, Egypt; nancy.saad@guc.edu.eg (N.H.); amr.elnemr@guc.edu.eg (A.E.-N.)

² Civil Engineering Department, Sherbrooke University, Sherbrooke, QC J1K 2R1, Canada

³ School of Computing and Engineering, University of West London, London W5 5RF, UK

* Correspondence: ibrahim.shaaban@uwl.ac.uk

Abstract: Alkali-activated slag (AAS) materials are one of the most promising sustainable construction composites. These novel materials are highly characterized by their improved mechanical and durability properties. Nevertheless, the high shrinkage rate hinders their full-scale applications. The low Ca/Si ratio, complex hydration process, and fine pore microstructure are the main causes of the reported shrinkage behavior. This study introduces *Bacillus subtilis* culture for healing the cracking behavior. The enzymatic action leads to precipitating calcium carbonate crystals that fill AAS cracks and pores. Incorporating calcium oxide has been recommended in multiple studies. The main purpose of adding calcium oxide is to enhance the engineering properties of AAS and provide more calcium ions for the biochemical reactions induced by the added bacteria. However, inconsistent findings about the influence of calcium oxide have been reported. This research provides further insights into the effect of calcium oxide (CaO) on the performance of microbial self-healing efficiency in AAS composite. The results highlight that incorporating calcium oxide as 7% of the binder partial replacement has an impact on the engineering properties of bio-AAS materials. The study recommends correlating the percentage of free calcium ions within the AAS mixture with the microbial activity.

Keywords: alkali-activated slag; self-healing; microbial self-healing; bacteria; *Bacillus subtilis*; calcium oxide



Citation: Hammad, N.; El-Nemr, A.; Shaaban, I.G. The Efficiency of Calcium Oxide on Microbial Self-Healing Activity in Alkali-Activated Slag (AAS). *Appl. Sci.* **2024**, *14*, 5299. <https://doi.org/10.3390/app14125299>

Academic Editor: Syed Minhaj Saleem Kazmi

Received: 10 May 2024

Revised: 10 June 2024

Accepted: 17 June 2024

Published: 19 June 2024



Copyright: © 2024 by the authors. Licensee MDPI, Basel, Switzerland. This article is an open access article distributed under the terms and conditions of the Creative Commons Attribution (CC BY) license (<https://creativecommons.org/licenses/by/4.0/>).

1. Introduction

One of the largest energy-consuming and air-polluting industries is the cement manufacturing process. Twelve to 15% of the overall energy consumed in the industry is directly related to cement production [1]. The annual cement production records 4.6 billion tons, with anticipation of reaching 6 billion tons by the end of 2025 [2,3]. On the other hand, the cement industry contributes to global greenhouse gas emissions by 12% [4,5]. Alkali-activated composites, or geopolymers, are introduced and recommended to replace Ordinary Portland Cement (OPC) concrete. They are presented as an environmentally friendly solution that proposes utilizing industrial by-products such as metallurgical slag or fly ash. In addition, they are characterized by their distinguished performance in terms of mechanical and durability properties [6,7]. Extensive research [8–10] has been devoted to investigating these sustainable materials. However, a high shrinkage rate is reported in multiple studies as one of the obstacles that hinders the full application of alkali-activated composites. The higher shrinkage rate of alkali-activated materials is associated with the finer pore microstructure and the complex hydration process. The percentage of mesopores in the alkali-activated composite systems is about 74–82%, compared to 24–36% in the OPC pastes [11,12]. Larger capillary tensile stresses are induced by finer pores, causing shrinkage cracks. The second reason is the formation of two categories of calcium silicate hydrates (C-S-H) gels. The higher surface area of slag leads to the formation of low-density

C-S-H and high-density C-S-H gels. The high percentage of low-density C-S-H gels and the reduced Ca/Si ratio in the alkali-activated systems (Ca/Si = 1.1) compared to that within the OPC (Ca/Si = 2) explain the shrinkage behavior. The shrinkage behavior is activated due to the continuous matrix re-arrangement that takes place at any humidity or moisture condition change [11–15]. A promising environmental repair approach called “microbial self-healing” has been developed and investigated for multiple engineering purposes. The microbial repair technology has shown promising results in healing cracks, and improving the mechanical and durability properties. The methodology of this sustainable application is dependent on the ureolytic action of the added bacteria [5,16–18]. The enzymatic hydrolyzation of urea increases the pH value, producing carbonate ions that form calcite precipitate in the presence of calcium ions. The calcite crystals fill the pores and cracks, enhancing the engineering properties [5,17,18].

Some studies have recommended incorporating calcium oxide to enhance the concrete’s self-healing property, as addressed in Table 1. Yildirim et al. [19] added CaO by 2.5% and 5% of the total binder to highlight the positive influence of CaO on the crack closure. Zhang et al. [4] proposed incorporating calcium oxide in alkali-activated mixtures by 7% of the total binder weight to provide more calcium ions that may motivate the self-healing property of the slag. Shahen et al. [20] completely replaced the binder with lime powder, confirming that CaO could facilitate microbe activity in the cementitious matrix. The addition of CaO has attracted the attention of multiple scholars [11,21–28] to adjust the Ca/Si ratio and improve the alkali-activated composite properties. However, a contradiction has been realized regarding the influence of CaO addition on the engineering properties of the alkali-activated materials. Table 2 indicates the scattered findings of some studies reporting the influence of CaO on the behavior of the alkali-activated material. Favorable evolution in mechanical properties has been reported in some cases [20]. Other findings have confirmed the negative effect of immobilizing calcium oxide on the mechanical properties of alkali-activated mixtures [19]. The common behavior that has been figured out is the decrease in flowability and the setting time with the addition of CaO. This could be explained by the high dissolution rate of the calcium and silicon ions within the matrix, which leads to an increase in the hydration heat. This could accelerate the hydration process, decreasing the setting time and flowability [24,26]. The high dissolution rate is accompanied by high medium alkalinity and a significant water consumption rate, which may cause a deterioration in the fresh and hardened properties [21]. The influence of the CaO addition on the mechanical property is mainly associated with the precursor type and chemical composition, the percentage of CaO, the alkaline activator type and concentration, and the curing conditions. Some scholars have attributed the enhancement in the mechanical properties to the better breaking and dissolution of the matrix atoms, providing a denser C-S-H gel. On the other hand, Chindaprasirt et al. explained the deterioration in the mechanical properties by the quick setting behavior. This behavior is associated with poor formwork that produces a destabilized C-A-S-H gel. Temuujin et al. [28] added that the higher hydration heat could lead to water evaporation, causing high porosity and reducing the compressive strength. This was supported by the findings of Burciaga-Díaz et al. [25] and Temuujin et al. [28], which emphasized that applying heat curing led to a reduction in mechanical properties due to water loss.

Based on the above discussion, the influence of CaO has not been fully clear on the performance of AAS, in particular composites incorporating healing agents. Further studies are required to assess the influence of calcium oxide on the microbial behavior of alkali-activated composites. The selection of the CaO percentage was 7% of the total binder weight, as highlighted by some studies based on its positive contribution to the development of mechanical properties [4,11,26]. The performance of the selected bacteria, “*Bacillus subtilis*”, could be explored by detecting the ability of the microbe to precipitate calcite crystals in AAS material incorporating 7% CaO of the binder weight. This could be conducted through an experimental investigation of the mechanical, durability, and microstructure properties. The mechanical properties were tested in terms of compressive and flexural

strengths. Absorption, porosity, chloride resistance, and surface electrical resistivity were investigated to gain insights into the durability performance of the microbial AAS mortar. Microstructure analysis was traced using a scanning electron microscope (SEM) alongside image energy-dispersive X-ray (EDX) analyses and X-ray diffraction (XRD).

Table 1. The influence of CaO on the self-healing mechanisms.

Precursor	% of CaO	Self-Healing Mechanism	Healing Agent	Influence	References
Blended cement-fly ash	2.5 and 5	Autogenous	Polyvinyl alcohol (PVA)	Enhanced the closure of crack openings	[19]
Slag	7	Autogenous	PVA	Improved crack self-healing ability	[4]
CaO	100	Autonomous	<i>Bacillus subtilis</i>	Preserved the survival of <i>Bacillus subtilis</i>	[20]

Table 2. The influence of CaO on the fresh and hardened properties of alkali-activated composites.

Precursor	% of CaO	Activator	Curing Condition	Mechanical Properties	Flowability	Setting Time	References
Slag	2.5, 5, and 10	NaOH and Na ₂ SiO ₃	Room	↑	↓	↓	[21]
Slag	15	NaOH and Na ₂ SiO ₃	Room	↓	-	-	[21]
Slag	7	Ca(OH) ₂	Room	↑	↑	-	[11]
Slag	10	Ca(OH) ₂	Room	↓	↓	↓	[11]
Slag	5, 10, and 15	NaOH and Na ₂ SiO ₃	Room	↓	-	-	[22]
Slag	2.5 and 5	Na ₂ CO ₃	-	↑	↓	↓	[23]
Slag	1–3	KOH and K ₂ SiO ₃	20 °C	↑	-	↓	[24]
Slag	6	CaO as sole activator	20 °C	↓	-	-	[25]
Slag	6	CaO as sole activator	60 °C	↓	-	-	[25]
Flyash	2.5, 5, and 7	NaOH and Na ₂ SiO ₃	Room	↑	↓	↓	[26]
Flyash	5, 10, and 15	NaOH and Na ₂ SiO ₃	Room	↓	-	-	[27]
Flyash	1, 3, and 5	NaOH and Na ₂ SiO ₃	20 °C	↑	-	↓	[28]
Flyash	1, 3, and 5	NaOH and Na ₂ SiO ₃	70 °C for 24 h	↓	-	↓	[28]

↓ decrease. ↑ increase.

2. Experimental Program

2.1. Materials

Ground granulated slag was used as an AAS precursor. The chemical composition of slag was identified by utilizing X-ray fluorescence, as presented in Table 3. The finesses and the specific gravity of slag were 4088 cm²/g and 2.80, respectively. Sodium hydroxide (NaOH) flakes and sodium meta-silicate (Na₂SiO₃) were used to activate the AAS precursor. A NaOH solution was prepared 24 h before AAS mixing by adopting 37.2% sodium hydroxide flakes and 62.5% water (480 gm of NaOH was dissolved in 1 L of water to provide a solution with a molarity of 12). The Na₂SiO₃ solution was composed of 27% sodium oxide, 30.01% silicon oxide, and 59.72% water. Calcium oxide was added in the form of powder with a percentage of 7% of the binder weight.

Table 3. Chemical composition of slag.

Oxides	%
SiO ₂	35.40
CaO	36.87
Al ₂ O ₃	17.40
MgO	6.83
MnO	0.26
Fe ₂ O ₃	1.4
MnO	0.35
TiO ₂	0.11
S	0.24
L.O.I	0.50

Bacillus species are classified as alkaliphile microbes. Alkaliphile species are capable of survival in harsh surroundings with high alkaline levels. The strains (Figure 1) were

prepared in a medium composed of 1% tryptone, 0.5% yeast extract, 1% NaCl, and 1.5% agar at 4 °C. Glassware and instrument sterilization was a crucial phase for preventing any contamination. For cell concentration preparation, a spectrophotometer was used to determine the optical bacteria density to develop a cell concentration of 10^5 cells/mL. The determinacy of subtilis absorbance was performed by a qualitative procedure involving the changes in OD600 (optical density measurement at 600 nm) of spore suspensions during germination. The solution of the bacteria was monitored every 24 h to obtain the OD600. After 48 h, the bacteria culture showed a 0.65 optical density that reached 1.1 OD600. At elevated pH (10.5), the growth profile of *Bacillus subtilis* was the fastest, indicating the best alkali-resistant behavior. To convert the optical density into CFU/mL, sub-culturing of a pure bacterial strain into young exponential cells is performed.



Figure 1. *Bacillus subtilis* culture.

OD and CFU/mL are measured, and repeated measurements are performed until obtaining 0.1 OD and the corresponding CFU/mL. A linearized standard curve was plotted for conversion. The characteristics of pure culture for *Bacillus subtilis* are given in Table 4.

Table 4. *Bacillus subtilis* pure culture characteristics.

Characteristics of <i>Bacillus subtilis</i>	Value
Growth medium	3
Incubation time	24 h
Subculture	30 days
Gram stain	Positive
shape	Rod
Oxygen demand	Facultative

2.2. AAS Mortar Manufacture

Alkaline solution blending was the first step in AAS manufacture. After blending the solutions, a certain water content was added according to the design steps. The design procedure was conducted by solving the equations of concrete absolute volume along with the equations of alkali dosage ($\text{Na}_2\text{O}\%$), modulus silicates (M_s), and liquid-to-binder ratio (L/b) simultaneously (Equations (1)–(4)) [29]. The ratio of slag to fine aggregate was kept at 1:3 based on the recommendations of the Egyptian Code of Practice (ECP 203) [30]. During the AAS mixing, solid constituents, including slag, calcium oxide powder, and fine aggregate, were perfectly mixed in a 5-L capacity Hobart mixer for 3 min (Figure 2a). After that, the liquid solutions were carefully added to the solid mixture for a further 2 min. For the microbial-induced AAS mixtures, *Bacillus subtilis* culture at a concentration of 10^5 cells/mL was gently added to the AAS mix in the form of the calculated water content as per volume. The mixing process continued for 2 min. Before the mixing process,

metallic molds were oiled and prepared for mortar pouring. Demoulding took place after 24 h of the AAS manufacturing process. A water curing regime at room temperature ($21\text{ }^{\circ}\text{C} \pm 2$) was applied for AAS specimens incorporating microbes for 7 and 28 days to provide an adequate environment for the microbes' survival (Figure 2b). To assess the bacteria's efficiency in healing cracks, the pre-cracking phase was considered for some specimens. Pre-cracking was carried out by subjecting AAS specimens to a compression load of 85% of their ultimate load capacities. For evaluating the crack healing progress, photo documentation was performed before and after subjecting the specimens to water curing to motivate the healing process.

$$\frac{\text{Slag}}{\text{SG}_{\text{slag}}} + \frac{\text{Na}_2\text{SiO}_3}{\text{SG}_{\text{Na}_2\text{SiO}_3}} + \frac{\text{NaOH}}{\text{SG}_{\text{NaOH}}} + \frac{\text{H}_2\text{O}}{\text{SG}_{\text{H}_2\text{O}}} = 1000 \text{ L} - \frac{\text{CA}}{\text{SG}_{\text{CA}}} - \frac{\text{FA}}{\text{SG}_{\text{FA}}} \quad (1)$$

where slag is the weight of slag content in kg, SG_x indicates the specific gravity of the corresponding material, x , Na_2SiO_3 shows the weight of sodium silicates in kg, NaOH is the weight of sodium hydroxide in kg, H_2O represents the weight of water in kg, CA is the coarse aggregates weight in kg, and FA shows fine aggregates weight in kg.

$$\text{Na}_2\text{O}\% = \frac{\text{Na}_2\text{O}\% \text{ in NaOH} + \text{Na}_2\text{O}\% \text{ in Na}_2\text{SiO}_3}{\text{Mass of slag}} \quad (2)$$

$$\text{Ms} = \frac{\text{SiO}_2\% \text{ in Na}_2\text{SiO}_3}{\text{Na}_2\text{O}\% \text{ in Na}_2\text{SiO}_3 + \text{Na}_2\text{O} \text{ in NaOH}} \quad (3)$$

$$\text{L/S} = \frac{\text{Water in all solutions}}{\text{Slag} + \text{Na}_2\text{O}\% \text{ solids} + \text{SiO}_2 \text{ solids}} \quad (4)$$

where $\text{Na}_2\text{O}\%$ in NaOH and $\text{Na}_2\text{O}\%$ in Na_2SiO_3 are the percentages of sodium oxide solids in the sodium hydroxide and sodium metasilicate solutions, respectively, $\text{SiO}_2\%$ in Na_2SiO_3 represents the percentage of silicon oxide solids in the sodium metasilicate solution. Water in all solutions indicates the percentage of water in the mixture.



(a)



(b)

Figure 2. AAS manufacturing process: (a) fresh mixing; (b) hardened AAS specimens.

To capture the influence of adding calcium oxide to the bio-AAS composites, three mixtures were adopted. The first mixture was the control AAS mix "C" without any bacteria or calcium oxide addition. The second category of mixes was the AAS mix with bacteria incorporation "C5". C5 indicates the bacteria concentration, which was 10^5 cells/mL. The final category of AAS mix included bacteria and the 7% calcium oxide addition "Ca-5". Ca-5 refers to including 7% calcium oxide along with incorporating bacteria with a concentration of 10^5 cells/mL. Table 5 illustrates the adopted AAS mixes in this study.

Table 5. AAS mixes proportions.

Mix ID	Slag kg/m ³	NaOH kg/m ³	Na ₂ SiO ₃ kg/m ³	H ₂ O kg/m ³	Na ₂ O%	Ms Ratio	L/B Ratio	Bacteria Concentration Cells/mL	CaO kg/m ³
C	387.40	60.45	82.81	81.61	8%	0.8	0.38	-	-
C5	387.40	60.45	82.81	81.61	8%	0.8	0.38	10 ⁵	-
Ca-5	359.60	60.45	82.81	81.61	8%	0.8	0.38	10 ⁵	27.80 (7%)

2.3. The Assessment Technique

2.3.1. Mechanical Property Testing

The mechanical properties were tested to assess the influence of incorporating CaO on the ability of *Bacillus subtilis* to precipitate calcium carbonate. Mechanical property evaluation, in particular compressive and flexural strength tests, was conducted on all AAS specimens after 7 and 28 days through the universal testing machine of capacity 2000 KN. Mortar cubes of 40 mm have been tested under compression at a pacing rate of 240 kg/m³ per minute according to the specifications of ASTM C109 [31] and ECP 203 [30]. Prisms of 40 × 40 × 160 mm were subjected to a three-point loading flexural test at the specified ages as per ASTM C348 [32] and ECP 203 [30]. Specimens were symmetrically placed between the two roller supports to have a center-to-center span length of 100 mm. The loading cell roller was placed in the midspan for applying the load at equal spaces from both supports. The rate of the applied load was about 50 N/s. The average of three separate specimens from each mixture and testing age were evaluated.

2.3.2. Durability Property Testing

The durability properties, including water absorption, porosity, chloride attack resistance, and surface electrical resistivity, were evaluated to check the effectiveness of bacteria in precipitating calcite crystals in the AAS specimens' pores. Specimens adopted for durability testing are cylindrical discs of 100 mm diameter and 50 mm thickness. Water absorption and porosity tests were performed according to ASTM C-642 [33]. All observations were taken in triplicate.

To assess the AAS mixtures, the Rapid Chloride Permeability Test (RCPT) was carried out on 28-day-old specimens following the specifications of ASTM C1202 [34] and AASHTO T277 [35]. The first specimens were placed in a vacuum desiccator. The vacuum pump was operated until the pressure reached less than 6650 Pa and was maintained for 3 h. After that, the funnel was filled with de-aerated water. Specimens were preserved underwater in an RCPT cell (without allowing air access) for 182 h. The rapid chloride permeability test started by applying a potential of 60 V across a circular disc of 100 mm diameter × 50 mm depth. The edges of all specimens were epoxy-coated. One end of the sample was immersed in sodium chloride (3% NaCl). The other side was placed in sodium hydroxide (0.3 M). A direct current was applied across the two sides, as highlighted in Figure 3a. The current passing through the specimen was recorded at a time interval of one minute for six hours, and the total charge in Coulombs was automatically computed. Based on the total charges passed, the chloride resistance was classified.

Surface electrical resistivity was determined by applying the four probe Wenner electrodes, as shown in Figure 3b. The electrical resistivity test was adopted by using the nondestructive "respond concrete resistivity meter". The Wenner electrodes were localized in an equal-spaced straight line. The external electrodes emitted an alternating current (AC) into the specimen, while the inner ones determined the electric potential produced. The specimens should have a 100% saturated surface and be dry during the testing for reliable electrical resistivity measurements. The resistivity was determined in kilohms-centimeters (kΩ-cm). As per AASHTO T358-15 [36], the surface resistivity could give a good indication of chloride ion penetration. Three cylindrical specimens with a 100 mm diameter and 200 mm length for each mix are recommended by AASTO T358-15 [36].

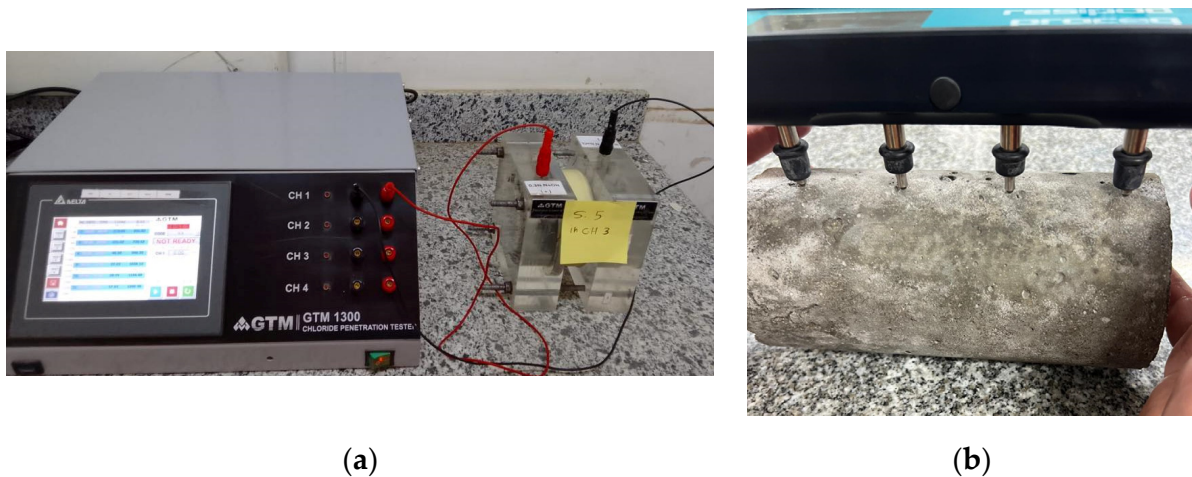


Figure 3. (a) The Rapid Chloride Permeability Test (RCPT) under testing cylinder specimen (b) The electrical resistivity of the concrete surface while measuring using the four-probe Wenner electrodes.

2.3.3. Microstructural Analysis

To capture the healing progress of the AAS specimens and check the ability of microbes to precipitate calcite crystals, scanning electron microscopy (SEM) was applied. Crushed powder specimens were scanned in an electron microscope equipped with an energy-dispersive X-ray analysis (EDX) detector. To explore the produced chemical compounds, such as hydration products and calcium carbonate precipitation, an X-ray diffraction test (XRD) was performed.

3. Results and Analysis

3.1. Mechanical Properties

Incorporating calcium oxide was proposed by previous researchers [4,37] to provide a highly alkaline environment that promoted the formation of C-S-H. Furthermore, it was expected that increasing the calcium ions in the matrix would enhance the biochemical reactions of the added bacteria, resulting in high calcium carbonate precipitation. The fact is that incorporating calcium hydroxide in the AAS mix had a negative influence on the compressive strength of the AAS mortar. A reduction in the compressive strength of 50.7% and 46.5% was observed after 7 and 28 days of curing, respectively, as presented in Figure 4a. These results are consistent with the findings of Lee et al. [38], who tested the influence of calcium oxide on the behavior of alkali-activated concrete composed of various binders. The concrete binder with the highest CaO (6.1% of its raw constituents) recorded the shortest setting time when calcium oxide was incorporated into the alkali-activated mixture. The final setting time significantly decreased as the molarity of the activator solution increased. Hence, insufficient time was available for the solid dissolution of the composites, including CaO. Subsequently, a remarkable reduction was recorded for the 7-day compressive strength. The addition of lime causes an instant precipitation of metal hydroxide that consumes more localized hydroxyl ions. Therefore, a sudden drop was marked in the pH level, triggering the chemical reactions and the polymerization process. If these conditions occur at a saturated level of silicate concentration, rapid silicate gelation will take place, producing larger particles with less surface energy [39,40]. This was confirmed by another study conducted by Seo et al. [22] that reported a reduction of 66% in the compressive strength after adding lime to AAS systems. It is worth noting that the speed of gel formation mainly depends on the nature of the added solids, activator compositions, and the species of dissolved ions [38,41].

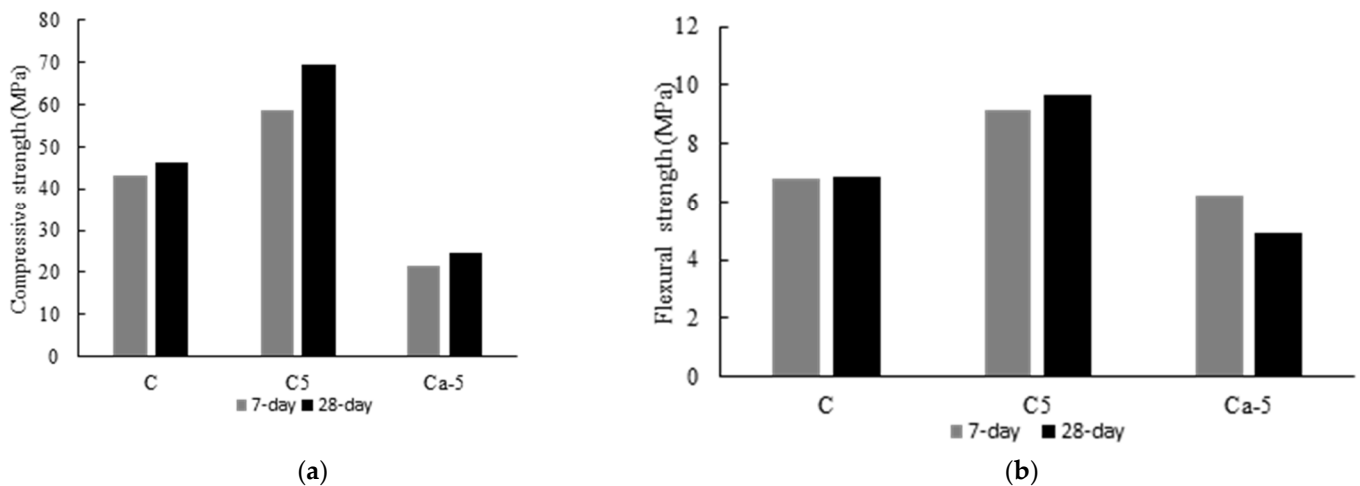
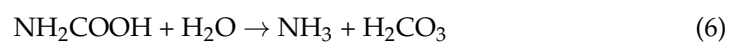


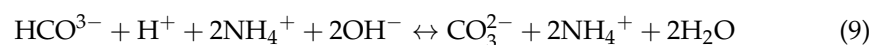
Figure 4. Mechanical properties testing results of AAS specimens after 7 and 28 days: (a) compressive strength, and (b) flexural strength.

The influence of incorporating bacteria was not significant for this type of mixture composition. The negative effect of incorporating calcium oxide was more pronounced when compared with the microbial influence. One of the important steps required for microbiological enzymatic ureolysis is the production of hydroxide ions. Hydroxide ions increase the pH level, which adjusts the overall equilibrium for precipitating calcium carbonate, as explained in the following Equations (5)–(11) [5]. Nevertheless, upon adding lime to the composite, most of the hydroxyl ions were consumed by calcium ions, disrupting the biochemical reaction series and reducing the microbial activity.

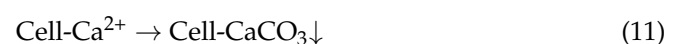
1. Hydrolyzing urea to produce carbonate and ammonia in the presence of urease, followed by a series of biological reactions to produce bicarbonate and hydroxide ions.



2. Hydroxide ions elevate the pH value, promoting the formation of carbonate ions.



3. An attraction force takes place between the positively charged calcium ions (Ca^{2+}) and the negatively charged carbonate ions (CO_3^{2-}), precipitating calcium carbonate (CaCO_3) at the cell surface.



Flexural strength behavior has a similar trend to compressive strength when calcium oxide is incorporated as a partial replacement (7%) of slag. A drop of 21.6% was observed in the value of 28-day flexural strength (4.86 MPa) concerning the control mix, as shown in Figure 4b. This is related to the increased amount of total shrinkage with time as a result of the increase in autogenous shrinkage, which imposes several pore structures inside the matrix. A study carried out by He et al. [39] and Fang et al. [40] on adding lime to an AAS composite activated by water glass demonstrated that the magnitude of autogenous shrinkage is directly affected by the percentage of the added lime

(see Figure 4 in [39] and Figure 6 in [40]). Autogenous shrinkage mainly appeared in the fresh state due to chemical shrinkage, which denoted the high reactivity and accelerated setting time of the mixture. Thus, the behavior of the composites varies in the hardened state, where the continuous rearrangement of the AAS matrix induces extra-autogenous shrinkage [42,43]. The remarkable decrease in the flexural strength upon adding CaO to the microbial AAS mix (from 9.65 MPa for C5 to 4.9 for Ca-5), as clear in Figure 4b, showed the possibility of introducing more CaO that helped in reacting with the water glass and inducing more autogenous shrinkage and pores at an early stage. Furthermore, the rapid setting time caused by the excessive amount of calcium led to a quick hydration process and fluidity loss that resulted in defects in the composite. Hexagonal portlandite crystals are formed immediately by incorporating lime into the mixture. The interface and the layered surface of the produced plate crystals are the main factors for the poorly developed mechanical properties [41]. This is explained clearly in Sections 3.3 and 3.4 when studying the microstructural behavior of a matrix.

3.2. Durability Properties

3.2.1. Water Absorption and Porosity

The reduction in the mechanical properties of C5 upon the addition of calcium oxide is explained by observing the results of water absorption and porosity tests, as illustrated in Figure 5a,b. Incorporating calcium oxide in C5 resulted in an increase in absorption and porosity of 54.9% and 26.2%, respectively. The high alkali content within the composite matrix had a substantial influence on accelerating the slag chemical bonds. At the same time, incorporating CaO increased the concentration of Ca^{2+} in the matrix. Therefore, the excessive amount of silicon and calcium led to the rapid formation of the silicate gel, producing larger particles [22,39–41]. Hence, the overlapping among the formed, large particles created larger spaces within the AAS composite. The presence of these voids was reflected in the water absorption and porosity tests. However, the increased values of water absorption and porosity were still lower than those exhibited by the control mix. This was linked to the microbial effect of partially filling the existing pores and generating new spaces, reducing the negative effect of the added calcium oxide.

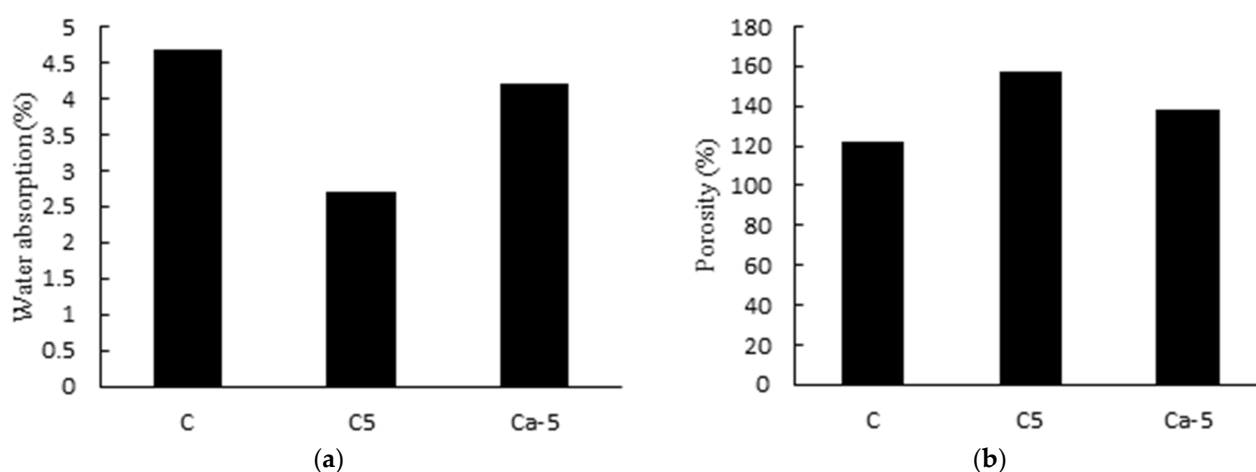


Figure 5. Physical properties of AAS specimens in terms of (a) water absorption and (b) porosity.

3.2.2. Rapid Chloride Permeability Test (RCPT)

It is important to highlight the factors influencing the results of the RCPT. RCPT is significantly affected by the microstructural properties of the concrete matrix in terms of pore structure, pore solution, chloride binding capacity, and phase evolution [13,44]. Pore distribution, pore continuity, and pore size have a pivotal role in transporting chloride ions. For instance, a smaller pore-size matrix is known to have higher chloride resistance [13,45]. The typical value of the pH level of AAS is 13.6, which is similar to that

of the OPC systems (13.28). Nevertheless, the pore solution of AAS completely differs from the OPC solution due to the excessive presence of Na^+ , OH^- , and HS^- . The presence of high OH^- along with a constant pH value enhances the stability and formation of C-A-S-H, reducing the Cl^-/OH^- ratio [44,45]. This reduced Cl^-/OH^- ratio improves the chloride resistance. However, it is worth mentioning that the high availability of mobile ions could reflect incorrect chloride resistance results due to the increase in charge conductivity. AAS systems have been reported to have lower binding chloride capacity, which was confirmed by the absence of chloro-aluminates (reaction between Cl^- and C_3A) in the XRD [46,47]. Based on the aforementioned factors, the automatic stoppage of the RCPT when applied to AAS mixtures could be explained. The increase in the ionic concentration by chloride penetration increases the mobility of the available free ions such as Na^+ , OH^- , and HS^- , reflecting false results about the passage of high electric charges.

The presence of calcium oxide in the bio-AAS specimens prolonged the testing time and increased the specimen resistance, as described in Table 6. The increase in the resistance time of Ca-5 compared to the mix incorporating bacteria only was mainly associated with the leaching and dissolving of more Ca^{2+} ions. Various reactions took place in the Ca-5 mixtures, consuming the mobile ions that might possess conductivity through the capillary pore structures of the AAS matrix. One of these reactions was the formation of hexagonal portlandite crystals [41]. In addition, anorthoclase ($\text{Na, K}(\text{SiAlO}_5)$) and albite ($\text{NaAlSi}_3\text{O}_8$) were detected in the XRD, as illustrated in Section 3.3. One more important reaction was the biomineralization reaction that occurred due to the enzymatic ureolysis effect of *Bacillus subtilis* [5]. Hence, the intensity of the mobile ions concerning C5 was reduced due to the reactions performed in the presence of Ca^{2+} ions. This finding is well supported by the results reported by Zhang et al. [4] about observing high electrical conductivity in RCPT testing of specimens incorporating lime. The increase in porosity in C and C-5 confronted the behavior postulated here, as the existence of high porosity allows the existence of alkali ions as Na^+ ions, which conduct electricity easily. Similarly, in Ca-5, however, some of these pores were plugged by the formation of calcium carbonate or more calcite.

Table 6. RCPT results of mixtures C, C5, and Ca-5.

	t (min)	0	30	60	90	120	150	180	210	240	270
C	Q (C)	260	919	1908	3253	-					
	I (A)	260	386	601	621						
C-5	Q (C)	124	443	777	1080	-					
	I (A)	138	177	185	168						
Ca-5	Q (C)	112	408	743	1122	1529	1970	2452	2970	3531	-
	I (A)	125	164	186	210	226	245	267	288	311	

Q: charges passed (Coulombs). I: current (amperes at "t" minutes after voltage started).

3.2.3. Surface Resistivity Test

The measured electrical resistivity could be directly correlated to the quality of concrete and its durability properties. The passage of the current is dependent on the concrete pores and their connectivity; the more well-connected pores exist, the more space and a better path for ion penetration. The average surface resistivity values measured were 122.2 k Ω -cm, 157.0 k Ω -cm, and 138.5 k Ω -cm for C, C5, and Ca-5, respectively (Figure 6). There is a clear consistency between the resistivity response results and the porosity behavior. Based on the specifications of AASHTO T358-15 that relate the resistivity results to chloride ion penetration, all the specimens showed very low chloride penetration. These results are more convenient with the nature of AAS systems, which are known for their high chloride attack resistance. The deviation between the results between the surface resistivity test and the RCPT could be attributed to heat generation during the RCPT and the associated high pore solution concentration that disrupts the process of measuring the actual chloride resistance in AAS systems.

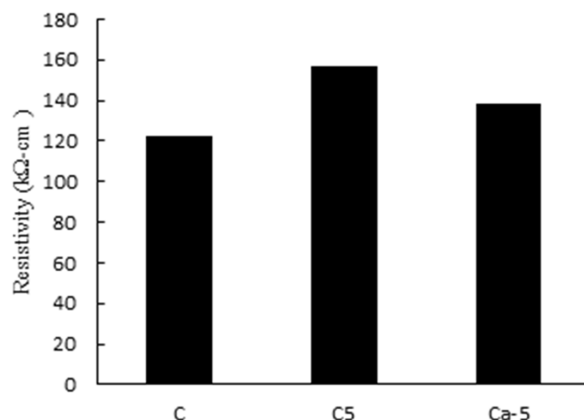


Figure 6. The electrical resistivity values of C, C5, and Ca-5.

3.3. XRD

Figure 7 indicates the formation of calcite within C5 and Ca-5, confirming the occurrence of the microbiological reactions within the AAS matrix. Calcium silicate hydrates (C-S-H) appeared to be more dominant in Ca-5 when compared to calcium aluminato silicate hydrates (C-A-S-H). The high leaching rate of Ca^{2+} ions in the AAS mix enhanced the formation of the hydration product C-S-H. Feldspar (KAlSi_3O_8) and relevant families, like anorthoclase ($(\text{Na}, \text{K})(\text{SiAlO}_5)$) and albite ($\text{NaAlSi}_3\text{O}_8$), were recognized in the XRD profile of Ca-5, which was not seen in the other AAS mixes. Ca^{2+} ions were highly detected in the formation of C-S-H and CaCO_3 , which linked the Feldspar together. Moreover, reactions took place between the other available ions, such as calcium, sodium, silicon, aluminum, oxygen, and potassium, forming an anorthoclase compound [48]. Since the formation of C-S-H became more dominant in this mix, the production of portlandite and calcite could be expected to link the feldspar together. Both of them are brittle and weak compounds that could be easily broken. Nevertheless, feldspar has a higher strength than calcite. Linking feldspar with calcite (CaCO_3) bicarbonate would weaken the resistance against flexural and bending loading. Thus, the decrease in the mechanical properties of Ca-5 could be associated with the formation of portlandite, which provided more spaces for crack propagation due to its large crystalline structure [48].

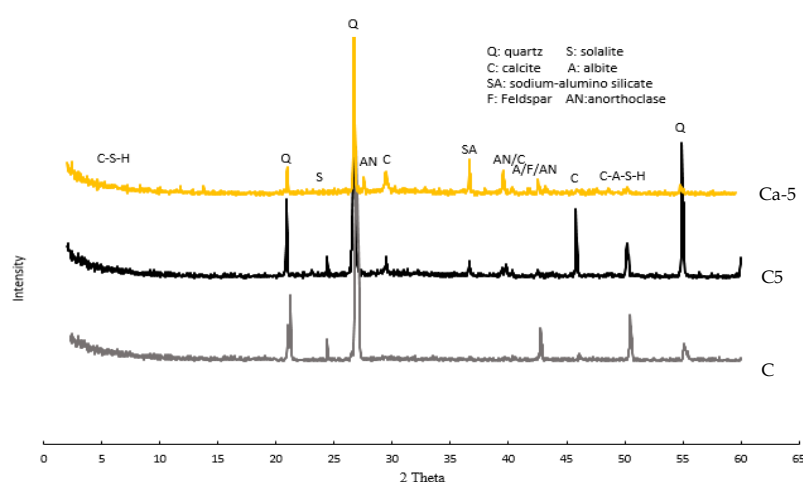


Figure 7. XRD of AAS mixtures C, C5, and Ca-5.

3.4. Microstructure Analysis

Multiple small particles were observed in the SEM of Ca-5 (Figure 8c). The shrinkage-induced cracks presented in the control mix seemed to be healed by dense-structure micro-crystals (Figure 8). The spectrum analysis of the EDX shows an abundant amount

of carbon content alongside the high content of calcium and oxygen, demonstrating the formation of a higher amount of calcium carbonate as well as confirming the microbial influence of *Bacillus subtilis*. Although the formed crystals filled the induced cracks, the overlap of the crystalline-formed structure appeared to have multiple voids within the matrix. The appearance of these weak points could cause a reduction in the developed strength and composite stiffness. The same results were reported by Nguyễn et al. [49] for AAS mixtures activated with calcium hydroxide. The detection of portlandite could be recognized within the microstructure. The carbon dioxide might be released during the curing process and react chemically with the produced portlandite to form calcite; however, the rapid setting time of Ca-5 might hinder this reaction from continuing [50]. The decrease in compressive strength with the increase in porosity becomes more convenient with the results presented by the microstructure of the AAS matrix.

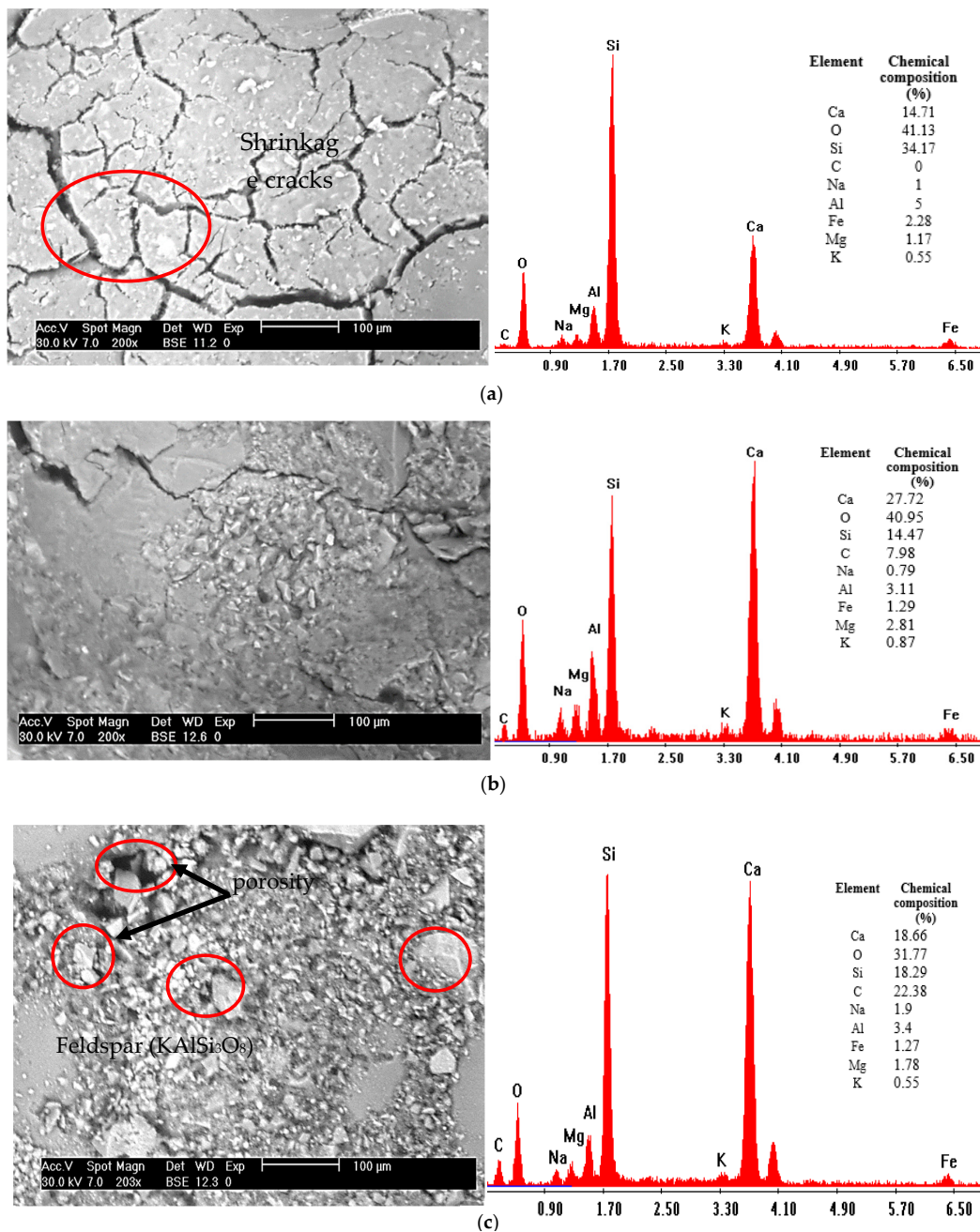


Figure 8. SEM images with EDX analysis of AAS mixtures (a) C, (b) C5, and (c) Ca-5.

3.5. Visualization of Surface Crack Healing

Although incorporating calcium oxide in the bio-AAS mixture led to a decrease in the mechanical properties, the treated Ca-5 specimens presented a good potential for crack width reduction and pore healing. The surface improvement included pore and crack healing, as illustrated in Figure 9. The results of the XRD confirmed the formation of calcium carbonate, which in turn reduced the water absorption and porosity when compared to the reference mixture. These findings are consistent with a previous study [4] on adding calcium carbonate to the AAS composite incorporating *Bacillus pasteurii*. The results highlighted the formation of calcium carbonate, which enhanced healing performance. However, a decrease in mechanical properties was mentioned due to the aforementioned reasons. However, the influence of bacteria on healing the cracks was much more substantial in the microbial AAS mix without calcium oxide.

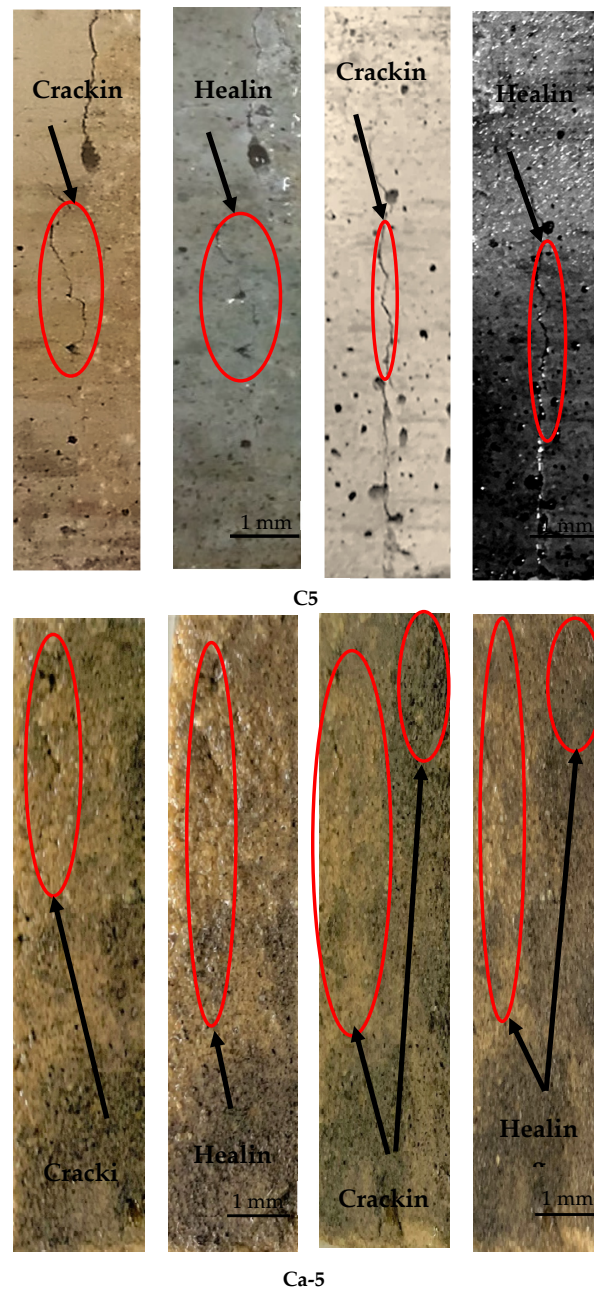


Figure 9. Visual observation of cracks before and after 28-day treatment with various biomixtures for C5 and Ca-5.

Figure 10 represents the crack width measured before and after implying the bacteria. The urealytic reaction of incorporating microbes into the AAS environment succeeded in precipitating calcite crystals within the crack's mouth. The formation of calcite could result in reducing the existing crack width from 1 mm to 0.3 mm in C5 specimens. Despite the severe Ca-5 matrix environment, *Bacillus subtilis* could proceed with the self-healing mechanism and fill in the crack width to achieve a maximum crack healing of about 80%.

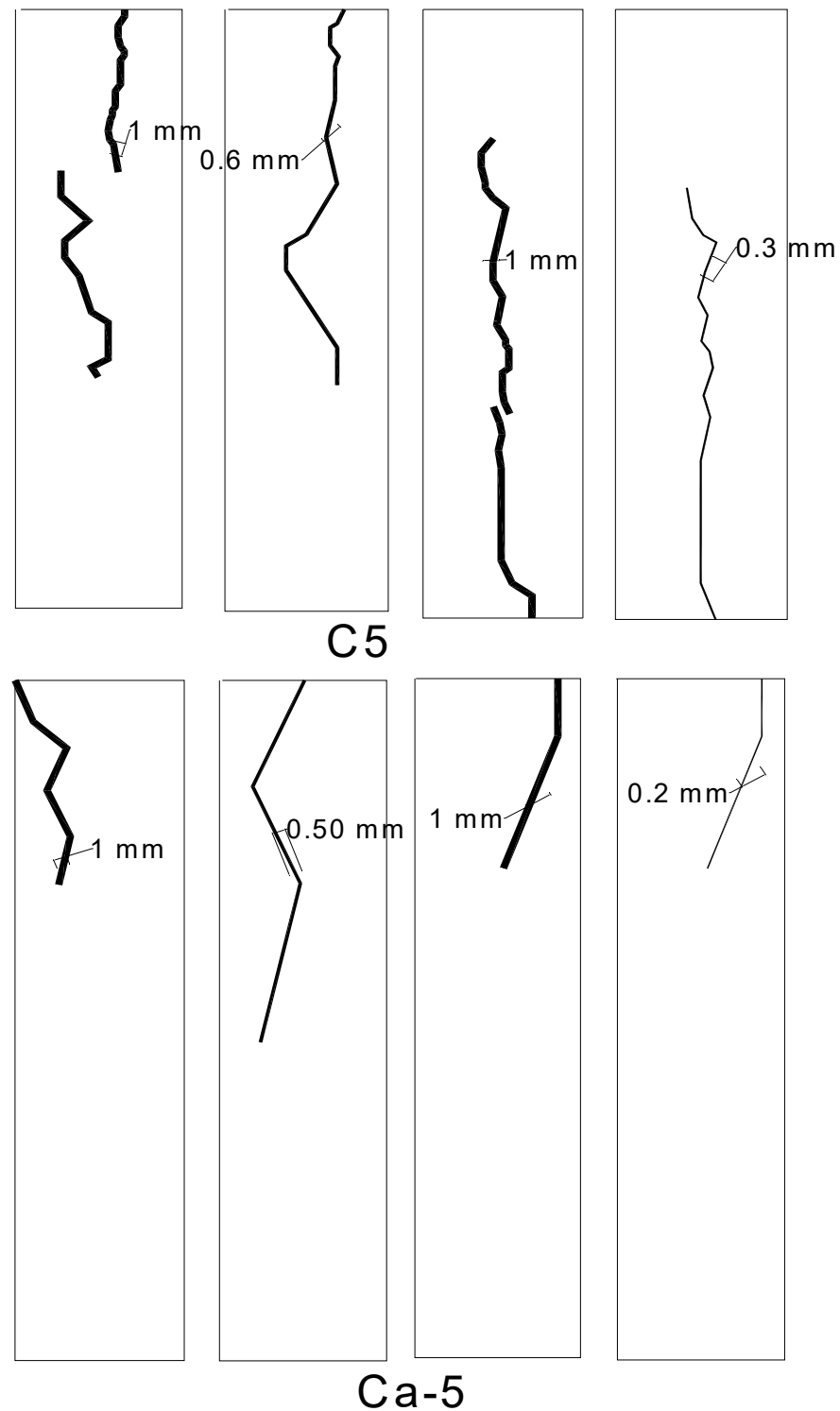


Figure 10. Healing of crack width observed before and after 28-day treatment of various biomixtures for C5 and Ca-5.

4. Conclusions

This study assessed the influence of calcium oxide on the ureolytic action of *Bacillus subtilis* within the AAS matrix. The assessment approach included mechanical property testing (compressive and flexural strengths), durability testing (water absorption, porosity, chloride resistance, and electric resistivity), and microstructural investigations through SEM, EDX, and XRD.

- The experimental evaluation indicated a deterioration in the mechanical properties of bio-AAS composites with calcium oxide incorporation, where a substantial drop (21.6%) in the mechanical properties was reported.
- Calcium oxide addition increased the free calcium ions that motivated the rapid formation of metal hydroxides. Metal hydroxide formation led to a reduction in the localized hydroxyl ions, disrupting the corresponding microbiological reactions of *Bacillus subtilis*.
- The presence of high silicate concentrations within these conditions resulted in instant silicate gelation with larger particle sizes. The overlapping between these larger particles created wider spaces, increasing the porosity of the composite.
- RCPT did not demonstrate the real chloride resistance of AAS mixtures because of the availability of mobile ions such as Na^+ , OH^- , and HS^- in addition to the Cl^- mobility. Incorporating CaO increased calcium ions that reacted with some of these available ions, reducing the passing charges and improving the RCPT results.
- The surface electrical resistivity proved the good chloride resistance of the AAS mixtures based on the classification of AASHTO T358-15.
- The results of the microstructure analysis highly illustrated the results observed during the mechanical and durability properties tests. However, CaO addition requires more investigation in the presence of microbial bacteria to determine the required concentration of calcium ions for optimum microbial efficiency.

Author Contributions: Methodology, N.H. and A.E.-N.; Validation, A.E.-N. and I.G.S.; Formal analysis, N.H.; Investigation, A.E.-N.; Writing—original draft, N.H.; Writing—review & editing, I.G.S.; Visualization, I.G.S.; Supervision, A.E.-N. and I.G.S.; Project administration, I.G.S. All authors have read and agreed to the published version of the manuscript.

Funding: This research received no external funding.

Institutional Review Board Statement: Not applicable.

Informed Consent Statement: Not applicable.

Data Availability Statement: The data presented in this study are available on request from the corresponding author.

Acknowledgments: Many thanks to the GUC laboratory, represented by the technician Ali Mohammed and the student Omar Naguib, who supported us while doing the experimental work.

Conflicts of Interest: The authors declare no conflicts of interest.

References

1. Hossain, M.U.; Poon, C.S.; Lo, I.M.; Cheng, J.C. Comparative LCA on using waste materials in the cement industry: A Hong Kong case study. *Resour. Conserv. Recycl.* **2017**, *120*, 199–208. [[CrossRef](#)]
2. Singh, G.B.; Subramaniam, K.V. Production and characterization of low-energy Portland composite cement from post-industrial waste. *J. Clean. Prod.* **2019**, *239*, 118024. [[CrossRef](#)]
3. Rashad, A.M. A Concise on the Effect of Calcium Oxide on the Properties of Alkali-Activated Materials: A Manual for Civil Engineers. *Int. J. Concr. Struct. Mater.* **2023**, *17*, 72. [[CrossRef](#)]
4. Zhang, L.V.; Suleiman, A.R.; Nehdi, M.L. Crack Self-Healing in NaOH-Activated Slag-Based Composites Incorporating Calcium Hydroxide. *J. Mater. Civ. Eng.* **2021**, *33*, 04021012. [[CrossRef](#)]
5. Hammad, N.; Elnemr, A.; Shaaban, I.G. State-of-the-Art Report: The Self-Healing Capability of Alkali-Activated Slag (AAS) Concrete. *Materials* **2023**, *16*, 4394. [[CrossRef](#)]

6. Hammad, N.; El-Nemr, A.; Hasan, H.E.-D. The performance of fiber GGBS based alkali-activated concrete. *J. Build. Eng.* **2021**, *42*, 102464. [[CrossRef](#)]
7. Shi, Z.; Shi, C.; Wan, S.; Zhang, Z. Effects of alkali dosage and silicate modulus on alkali-silica reaction in alkali-activated slag mortars. *Cem. Concr. Res.* **2018**, *111*, 104–115. [[CrossRef](#)]
8. Amer, I.; Kohail, M.; El-Feky, M.S.; Rashad, A.; Khalaf, M.A. A review on alkali-activated slag concrete. *Ain Shams Eng. J.* **2021**, *12*, 1475–1499. [[CrossRef](#)]
9. Mastali, M.; Kinnunen, P.; Dalvand, A.; Firouz, R.M.; Illikainen, M. Drying shrinkage in alkali-activated binders—A critical review. *Constr. Build. Mater.* **2018**, *190*, 533–550. [[CrossRef](#)]
10. Hammad, N.; ElNemr, A.M.; Hassan, H.E.-D. Flexural performance of reinforced Alkali-activated concrete beams incorporating steel and structural Macro synthetic polypropylene fiber. *Constr. Build. Mater.* **2022**, *324*, 126634. [[CrossRef](#)]
11. Yang, L.Y.; Jia, Z.J.; Zhang, Y.M.; Dai, J.G. Effects of nano-TiO₂ on strength, shrinkage and microstructure of alkali activated slag pastes. *Cem. Concr. Compos.* **2015**, *57*, 1–7. [[CrossRef](#)]
12. Zhang, B.; Zhu, H.; Cheng, Y.; Huseien, G.F.; Shah, K.W. Shrinkage mechanisms and shrinkage-mitigating strategies of alkali-activated slag composites: A critical review. *Constr. Build. Mater.* **2022**, *318*, 125993. [[CrossRef](#)]
13. Ye, H.; Radlińska, A. Shrinkage mitigation strategies in alkali-activated slag. *Cem. Concr. Res.* **2017**, *101*, 131–143. [[CrossRef](#)]
14. Cartwright, C.; Rajabipour, F.; Radlińska, A. Shrinkage Characteristics of Alkali-Activated Slag Cements. *J. Mater. Civ. Eng.* **2015**, *27*, B4014007. [[CrossRef](#)]
15. Li, Z.; Nedeljković, M.; Chen, B.; Ye, G. Mitigating the autogenous shrinkage of alkali-activated slag by metakaolin. *Cem. Concr. Res.* **2019**, *122*, 30–41. [[CrossRef](#)]
16. Hassanin, A.; El-Nemr, A.; Shaaban, H.F.; Saidani, M.; Shaaban, I.G. Coupling Behavior of Autogenous and Autonomous Self-Healing Techniques for Durable Concrete. *Int. J. Civ. Eng.* **2024**, *22*, 925–948. [[CrossRef](#)]
17. Jadhav, U.U.; Lahoti, M.; Chen, Z.; Qiu, J.; Cao, B.; Yang, E.-H. Viability of bacterial spores and crack healing in bacteria-containing geopolymer. *Constr. Build. Mater.* **2018**, *169*, 716–723. [[CrossRef](#)]
18. Jogi, P.K.; Lakshmi, T.V. Self healing concrete based on different bacteria: A review. *Mater. Today Proc.* **2020**, *43*, 1246–1252. [[CrossRef](#)]
19. Yildirim, G.; Sahmaran, M.; Ahmed, H.U. Influence of Hydrated Lime Addition on the Self-Healing Capability of High-Volume Fly Ash Incorporated Cementitious Composites. *J. Mater. Civ. Eng.* **2015**, *27*, 04014187. [[CrossRef](#)]
20. Shaheen, N.; Khushnood, R.A.; Din, S.U.; Khalid, A. Influence of bio-immobilized lime stone powder on self-healing behaviour of cementitious composites. *IOP Conf. Series Mater. Sci. Eng.* **2018**, *431*, 062002. [[CrossRef](#)]
21. Gharieb, M.; Rashad, A.M. Impact of sugar beet waste on strength and durability of alkali-activated slag cement. *ACI Mater. J.* **2022**, *119*, 79–90. [[CrossRef](#)]
22. Seo, J.; Kim, S.; Park, S.; Bae, S.J.; Lee, H.K. Microstructural evolution and carbonation behavior of lime-slag binary binders. *Cem. Concr. Compos.* **2021**, *119*, 104000. [[CrossRef](#)]
23. Chen, Z.; Ye, H. The role of CaO and MgO incorporation in chloride resistance of sodium carbonate-activated slag. *Cem. Concr. Compos.* **2022**, *132*, 104625. [[CrossRef](#)]
24. Ju, C.; Liu, Y.; Jia, M.; Yu, K.; Yu, Z.; Yang, Y. Effect of calcium oxide on mechanical properties and microstructure of alkali-activated slag composites at sub-zero temperature. *J. Build. Eng.* **2020**, *32*, 101561. [[CrossRef](#)]
25. Burciaga-Díaz, O.; Betancourt-Castillo, I.; Montes-Escobedo, M.; Escalante-García, J. One-part pastes and mortars of CaO-Na₂CO₃ activated blast furnace slag: Microstructural evolution, cost and CO₂ emissions. *Constr. Build. Mater.* **2023**, *368*, 130431. [[CrossRef](#)]
26. Rashad, A.M.; Gharieb, M. Solving the perpetual problem of imperative use heat curing for fly ash geopolymer cement by using sugar beet waste. *Constr. Build. Mater.* **2021**, *307*, 124902. [[CrossRef](#)]
27. Chindaprasirt, P.; Phoo-Ngernkham, T.; Hanjitsuwan, S.; Horpibulsuk, S.; Poowancum, A.; Injorhor, B. Effect of calcium-rich compounds on setting time and strength development of alkali-activated fly ash cured at ambient temperature. *Case Stud. Constr. Mater.* **2018**, *9*, e00198. [[CrossRef](#)]
28. Temuujin, J.; van Riessen, A.; Williams, R. Influence of calcium compounds on the mechanical properties of fly ash geopolymer pastes. *J. Hazard. Mater.* **2009**, *167*, 82–88. [[CrossRef](#)]
29. Hassan, A.; ElNemr, A.; Goebel, L.; Koenke, C. Effect of hybrid polypropylene fibers on mechanical and shrinkage behavior of alkali-activated slag concrete. *Constr. Build. Mater.* **2024**, *411*, 134485. [[CrossRef](#)]
30. ECP 203-2007; Egyptian Code for Design and Construction of Reinforced Concrete Structures, Design of Concrete Mixes. ECP: Islamabad, Pakistan, 2007.
31. ASTM C109; Standard Test Method of Compressive Strength of Hydraulic Cement Mortars (Using 2-in. or [50 mm] Cube specimens), Annual Book of ASTM Standard. ASTM International: West Conshohocken, PA, USA, 2020.
32. ASTM C348-21; Standard Test Method for Flexural Strength of Hydraulic-Cement Mortars, Annual Book of ASTM Standard. ASTM International: West Conshohocken, PA, USA, 2021.
33. ASTM C642-21; Standard Test Method for Density, Absorption, and Voids in Hardened Concrete, Annual Book of ASTM Standard. ASTM International: West Conshohocken, PA, USA, 2022.
34. ASTM C1202-19; Standard Test Method for Electrical Indication of Concrete's Ability to Resist Chloride Ion Penetration, Annual Book of ASTM Standard. ASTM International: West Conshohocken, PA, USA, 2022.

35. AASHTO-T277; Standard Method of Test for Electrical Indication of Concrete's Ability to Resist Chloride Ion Penetration. AASHTO: Washington, DC, USA, 2023.
36. AASHTO-T358; Standard Method of Test for Surface Resistivity Indication of Concrete's Ability to Resist Chloride Ion Penetration. AASHTO: Washington, DC, USA, 2019.
37. Dombrowski, K.; Buchwald, A.; Weil, M. The influence of calcium content on the structure and thermal performance of fly ash based geopolymers. *J. Mater. Sci.* **2007**, *42*, 3033–3043. [[CrossRef](#)]
38. Lee, W.; van Deventer, J. The effect of ionic contaminants on the early-age properties of alkali-activated fly ash-based cements. *Cem. Concr. Res.* **2002**, *32*, 577–584. [[CrossRef](#)]
39. He, J.; Bai, W.; Zheng, W.; He, J.; Sang, G. Influence of hydrated lime on mechanical and shrinkage properties of alkali-activated slag cement. *Constr. Build. Mater.* **2021**, *289*, 123201. [[CrossRef](#)]
40. Fang, G.; Bahrami, H.; Zhang, M. Mechanisms of autogenous shrinkage of alkali-activated fly ash-slag pastes cured at ambient temperature within 24 h. *Constr. Build. Mater.* **2018**, *171*, 377–387. [[CrossRef](#)]
41. Xiang, J.; Liu, L.; Cui, X.; He, Y.; Zheng, G.; Shi, C. Effect of limestone on rheological, shrinkage and mechanical properties of alkali-Activated slag/fly ash grouting materials. *Constr. Build. Mater.* **2018**, *191*, 1285–1292. [[CrossRef](#)]
42. Adam, A.A.; Amiri, N.H.; Suarnita, I.W.; Rupang, N. The Effect of Lime Addition on the Setting Time and Strength of Ambient Cured Fly Ash Based Geopolymer Binder. *MATEC Web Conf.* **2016**, *47*, 01015. [[CrossRef](#)]
43. Harutyunyan, V.S.; Kirchheim, A.P.; Monteiro, P.J.M.; Aivazyan, A.P.; Fischer, P. Investigation of early growth of calcium hydroxide crystals in cement solution by soft X-ray transmission microscopy. *J. Mater. Sci.* **2009**, *44*, 962–969. [[CrossRef](#)]
44. Zhang, J.; Ma, Y.; Hu, J.; Wang, H.; Zhang, Z. Review on chloride transport in alkali-activated materials: Role of precursors, activators and admixtures. *Constr. Build. Mater.* **2022**, *328*, 127081. [[CrossRef](#)]
45. Mundra, S.; Bernal, S.A.; Criado, M.; Hlaváček, P.; Ebell, G.; Reinemann, S.; Gluth, G.J.; Provis, J. Steel corrosion in reinforced alkali-activated materials. *RILEM Tech. Lett.* **2017**, *2*, 33–39. [[CrossRef](#)]
46. Lee, N.K.; Lee, H.K. Influence of the slag content on the chloride and sulfuric acid resistances of alkali-activated fly ash/slag paste. *Cem. Concr. Compos.* **2016**, *72*, 168–179. [[CrossRef](#)]
47. Ismail, I.; Bernal, S.A.; Provis, J.L.; Nicolas, R.S.; Brice, D.G.; Kilcullen, A.R.; Hamdan, S.; van Deventer, J.S. Influence of fly ash on the water and chloride permeability of alkali-activated slag mortars and concretes. *Constr. Build. Mater.* **2013**, *48*, 1187–1201. [[CrossRef](#)]
48. García-Lodeiro, I.; Fernández-Jiménez, A.; Palomo, A. Cementos híbridos de bajo impacto ambiental: Reducción del factor clinker. *Rev. Alconpat* **2015**, *5*, 1–17. [[CrossRef](#)]
49. Nguyễn, H.H.; Choi, J.-I.; Kim, H.-K.; Lee, B.Y. Effects of the type of activator on the self-healing ability of fiber-reinforced alkali-activated slag-based composites at an early age. *Constr. Build. Mater.* **2019**, *224*, 980–994. [[CrossRef](#)]
50. Khushnood, R.A.; Qureshi, Z.A.; Shaheen, N.; Ali, S. Bio-mineralized self-healing recycled aggregate concrete for sustainable infrastructure. *Sci. Total. Environ.* **2020**, *703*, 135007. [[CrossRef](#)]

Disclaimer/Publisher's Note: The statements, opinions and data contained in all publications are solely those of the individual author(s) and contributor(s) and not of MDPI and/or the editor(s). MDPI and/or the editor(s) disclaim responsibility for any injury to people or property resulting from any ideas, methods, instructions or products referred to in the content.